Journal of Power Sources 183 (2008) 730–740

Contents lists available at ScienceDirect

Journal of Power Sources

journal homepage: www.elsevier.com/locate/jpowsour

Fabrication and characterization of three-dimensional carbon electrodes for lithium-ion batteries

Genis Turon Teixidor*, Rabih B. Zaouk, Benjamin Y. Park, Marc J. Madou

Department of Mechanical and Aerospace Engineering, 4200 Engineering Gateway Building, University of California, Irvine, Irvine, CA 92697, USA

ARTICLE INFO

Article history:
Received 12 April 2008
Received in revised form 15 May 2008
Accepted 20 May 2008
Available online 7 July 2008

Keywords:
Carbon-MEMS
Lithium-ion batteries
MCMB
Three-dimensional electrode arrays
Microbattery

ABSTRACT

This paper presents fabrication and testing results of three-dimensional carbon anodes for lithium-ion batteries, which are fabricated through the pyrolysis of lithographically patterned epoxy resins. This technique, known as Carbon-MEMS, provides great flexibility and an unprecedented dimensional control in shaping carbon microstructures. Variations in the pattern density and in the pyrolysis conditions result in anodes with different specific and gravimetric capacities, with a three to six times increase in specific capacity with respect to the current thin-film battery technology. Newly designed cross-shaped Carbon-MEMS arrays have a much higher mechanical robustness (as given by their moment of inertia) than the traditionally used cylindrical posts, but the gravimetric analysis suggests that new designs with thinner features are required for better carbon utilization. Pyrolysis at higher temperatures and slower ramping up schedules reduces the irreversible capacity of the carbon electrodes. We also analyze the addition of Meso-Carbon Micro-Beads (MCMB) particles on the reversible and irreversible capacities of new three-dimensional, hybrid electrodes. This combination results in a slight increase in reversible capacity and a big increase in the irreversible capacity of the carbon electrodes, mostly due to the non-complete attachment of the MCMB particles.

1. Introduction

Even though the capabilities of portable electronic devices have experienced tremendous progress during the last decades, the need for small-scale power sources has not been successfully fulfilled and remains as one of the challenges for the miniaturization trend to continue. Lithium-ion batteries, based on the intercalation of lithium ions between an insertion cathode (e.g., $LiMn_2O_4$) and an insertion anode (e.g., carbon), are the most widely used power source for portable consumer electronics [1]. These types of batteries, operating at room temperature, offer several advantages with respect to conventional aqueous battery technologies: higher energy density (up to 160 Wh kg^{-1}, 300 Wh L^{-1}), higher cell voltage (3.7 V), longer shelf life (5–10 years), extended cyclability (1000–3000 cycles) and no memory effect [2], but their miniaturization remains a technological challenge. In microbatteries, the achievable power and energy densities do not scale down favorably because packaging and the internal battery hardware determine the overall size and mass of the battery to a large extent, but several approaches have been examined to this date, thin-film batteries being one of the more promising technologies [3]. In a thin-film solid state battery the layered materials are deposited by sputtering or evaporation, and the deposited battery stack, from current collector to anode, is less than 5 μm thick [4]. Although this technology has several advantages, such as high cyclability, total solid state construction, ability to operate between a wide range of temperatures (−20 to 140 °C) and customizable battery shapes and sizes, the total energy capacity remains in the order of tens of μAh cm^{-2}, which is not sufficient for most current applications. Besides, the cost per unit of energy delivered by thin-film batteries is several orders of magnitude higher than that of traditional batteries due to the use of high vacuum systems for the thin-film deposition process.

One possible solution to overcome the energy storage deficiencies in current microbatteries is to develop new architectures in which the electrode materials are reorganized into three-dimensional (3D) arrangements. In this new approach, the main objective is to maximize energy and power densities within the footprint area of the batteries while keeping short ionic transport distances. This is achieved by reconfiguring the electrodes in complex geometries, either in periodic arrays or non-uniform arrangements. As it has been already published, three-dimensional battery architectures present a larger energy capacity than traditional designs, up to 350% for the same areal footprint [5].

* Corresponding author. Tel.: +1 949 824 4143; fax: +1 949 824 8585.
E-mail addresses: gturonte@uci.edu (G.T. Teixidor), rzaouk@uci.edu (R.B. Zaouk), bypark@uci.edu (B.Y. Park), mmadou@uci.edu (M.J. Madou).

0378-7753/$ – see front matter © 2008 Elsevier B.V. All rights reserved.
doi:10.1016/j.jpowsour.2008.05.065

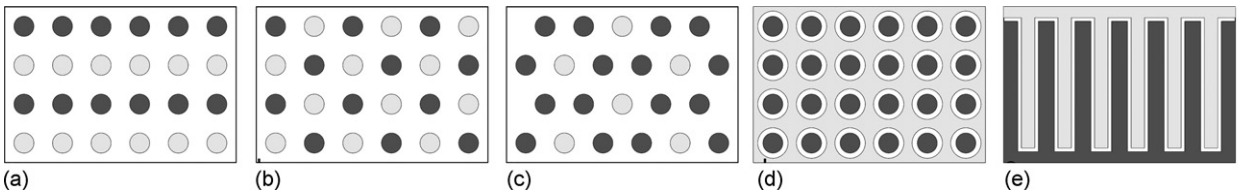

Fig. 1. Cross-sectional views of three-dimensional battery architectures: (a) parallel, (b) alternating, (c) hexagonal and (d) interpenetrating; dark gray: cathode, gray: anode, white: electrolyte. Adapted from Ref. [5] (e) side view of the interpenetrating design shown in (d).

Several methods have been used for the fabrication of three-dimensional carbon electrode arrays [6,7], but our approach is based on the pyrolysis of lithographically patterned photoresists. This process, pioneered by Madou et al. and named Carbon-microelectromechanical systems, or Carbon-MEMS [8], uses photolithography to pattern the polymeric precursors into the appropriate geometries. By controlling the parameters of the pyrolysis process it is possible to adjust the final properties of the resulting carbonaceous material.

2. Design implementation of the Carbon-MEMS anodes

While several possible configurations for three-dimensional battery designs have been discussed in the literature (for a comprehensive review, see Ref. [5]), an interpenetrating arrangement of the anode and cathode materials, separated by a thin, conformal electrolyte is one of the most promising. This design presents several advantages over parallel, alternating or hexagonal dispositions (see Fig. 1), such as a better utilization of the available volume (it minimizes the amount of non-active material) and a more facile manufacturing scheme (anode, cathode and electrolyte can be formulated separately). In order to obtain the high areal energy capacity that drives the interest in three-dimensional designs, the objective is to maximize the amount of carbon per footprint area. Therefore, high-aspect ratio microstructures are required (we define the aspect ratio as the height divided by the cross-sectional minimum feature; typical aspect ratios in our designs are >10:1). In their final configuration, Carbon-MEMS based three-dimensional carbon anodes consist of an underlying carbon layer with high-aspect ratio carbon structures patterned over it.

The initial three-dimensional carbon structures had a circular cross-section, which resulted in the aggregation of the pillars due to capillary effects resulting from Laplace pressure differences and surface tension forces [9]. One possible solution to overcome this problem is to use critical point drying methods [10], but since they are expensive and time-consuming processes, they are not suitable for a battery mass production setup. Instead, we have developed new geometries that have a higher area moment of inertia while maintaining short diffusion paths for lithium-ion intercalation. Out of several candidate geometries, a cross-shaped design has been chosen. To demonstrate the advantage of the new geometries, we can suppose a dimension d constant in both designs (see Fig. 2A). The moment of inertia in the principal directions for each design is

- cross-shape: $I_{cr} = 29/12d^4 \approx 2.42d^4$;
- cylindrical shape: $I_{cl} = \pi/64d^4 \approx 4.91 \times 10^{-2}d^4$

which gives $I_{cr} > I_{cl}$ for any given d, with a difference of two orders of magnitude. At the same time, by keeping d the same in both the old (cylinder) and the new (cross) designs we ensure that the diffusion distance for lithium ions remains approximately the same in both. Indeed, we can see that the new designs are clearly superior in terms of array uniformity after the fabrication process (see Fig. 2B and C).

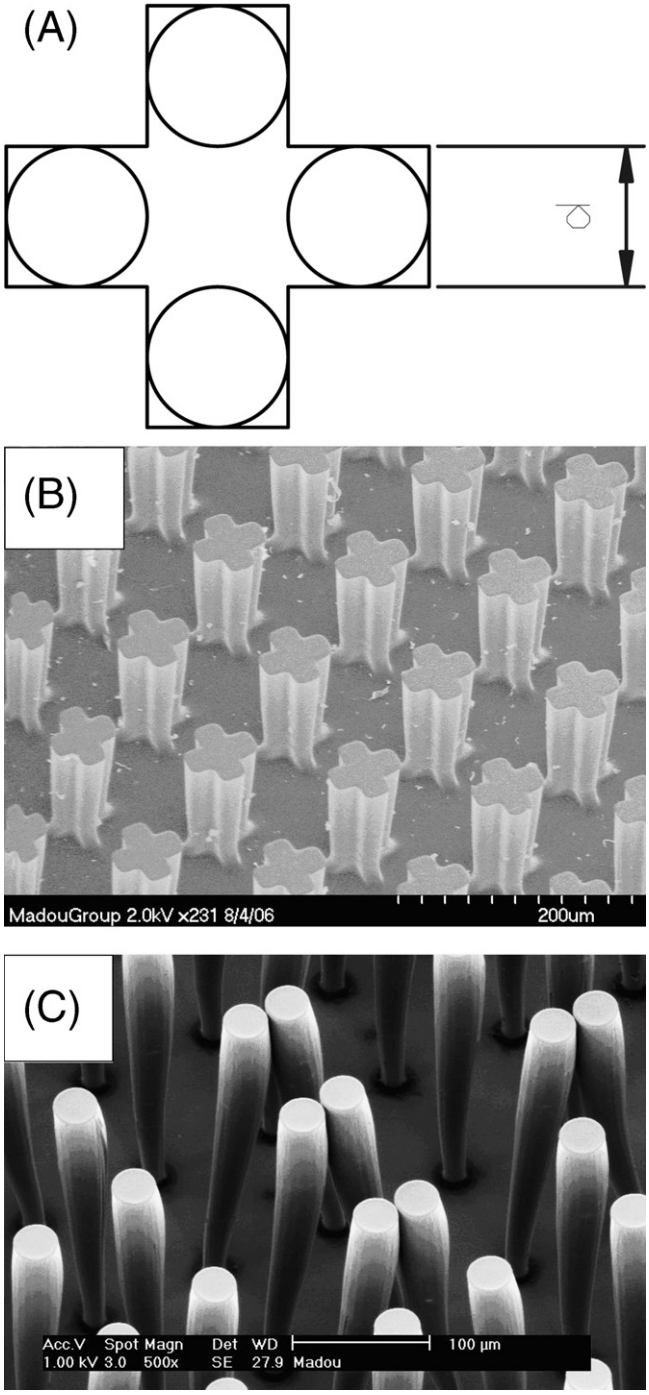

Fig. 2. (A) Cross-sectional shape of the new designs. Inside, the initial circular cross-sections, (B) arrays of cross-shaped electrodes and (C) initial cylindrical design.

Table 1
SU-8 processing parameters

Process name	First layer (SU-8(10))	Second layer (SU-8(100))
Spin coat	35 s at 3000 rpm (10 μm)	35 s at 1500 rpm (200 μm)
Soft bake	7 min at 95 °C (oven)	90 min at 95 °C (leveled hot plate)
Exposure dose	300 mJ cm^{-2} (flood exposure)	700 mJ cm^{-2} (using a mask)
Post-exposure bake	4 min at 95 °C (oven)	25 min at 95 °C (leveled hot plate)
Develop	N/A	25 min in 1-ethoxy-2-propyl acetate

3. Experimental

3.1. Carbon-MEMS processing

To fabricate the Carbon-MEMS three-dimensional anodes, the precursor of choice is SU-8 (Microchem Corp., MA), a chemically amplified negative tone photoresist based on epoxy-novolac resin designed for micromachining and other microelectronic applications. This photoresist is based on three components; an EPON epoxy resin, an organic solvent, and a photoinitiator [11]. The chemical formula of EPON resin SU-8 is a multifunctional glycidyl ether derivative of bisphenol-A novolac used to provide high-resolution patterning for semiconductor devices. The second component is gamma-butyrolactone (GBL), an organic solvent; the quantity of the solvent determines the viscosity of the solvent, which in turn determines final thickness of the spin-coated film. The third one is a triarylium–sulfonium salt (CYRACURE® UVI from Union Carbide), a photoinitiator which is approximately 10 wt.% of EPON SU-8. Epoxy resins are cationically polymerized by utilizing a photoinitiator which generates strong acid upon exposure to ultraviolet light (365–436 nm) and the acid facilitates polymeric cross-linking during post-exposure bake.

Upon pyrolysis under a reducing (i.e., oxygen-free) environment, the photoresist becomes a hard carbon due to its highly cross-linked molecular structure. Elemental analysis of pyrolyzed photoresists shows that the oxygen to carbon ratio is 0.06 for carbon films pyrolyzed between 800 and 1100 °C [12]. Furthermore, the crystalline structure of the material resulting from this process is comparable to commercial glassy carbon [13]. Hard carbons usually deliver capacities beyond that of the typical of graphitic carbons [14]. In this sense, hard carbons can be a powerful candidate for a lithium-ion battery anode material. Their ideal capacity exceeds that of graphite (450 mAh g^{-1} of hard carbons vs. 372 mAh g^{-1} for graphite [14]). The drawbacks are a higher irreversible capacity and occasionally a higher de-intercalation voltage. Specific conductivities and shrinkage rates of SU-8 derived carbons as well as their use in lithium batteries have been already reported [15,16].

In order to achieve the structures depicted in Fig. 2B, a two-layer process is used. The first layer results in the underlying carbon film and the second one in the three-dimensional structures. Therefore, two different formulations of the SU-8 photoresist are used: SU-8(10) and SU-8(100). The substrates used in the experiments are silicon wafers with a 5000-Å layer of SiO_2 (Noel Technologies, CA) which insulates the carbon from the conductive silicon substrate. The detailed process parameters for the fabrication of the polymer precursor structures are described in Table 1.

3.2. Combined C-MEMS/MCMB electrodes

One type of carbon commonly used in the fabrication of anodes for lithium-ion batteries is meso-carbon micro-beads, or MCMB, a very well graphitized carbon derived from pyrolysis at 2800 °C of coal tars or naphthalene precursors. MCMB electrodes are very stable upon cycling and can deliver an average reversible lithium storage capacity up to 325 mAh g^{-1} [17], relatively close to the maximum theoretical capacity of graphite (372 mAh g^{-1} [18]), and represent an industrial benchmark for the lithium-ion battery industry. In order to improve the total capacity and the intercalation reaction kinetics of the carbon anodes, we have fabricated a hybrid electrode consisting of Carbon-MEMS microstructures coated with MCMB particles. Our hypothesis was that such a hybrid electrode would have the enhanced areal capacity of three-dimensional electrodes while retaining the favorable cyclability and fast kinetics for Li^+ insertion of MCMB. Besides, coating carbon microstructures with MCMB is a unique method to obtain new carbon electrodes with superior mechanical stability and material homogeneity as compared to other approaches, such as filling micromachined silicon molds with electrode materials by colloidal processing methods [6]. An SEM image of the resulting hybrid electrodes is shown in Fig. 3A and B.

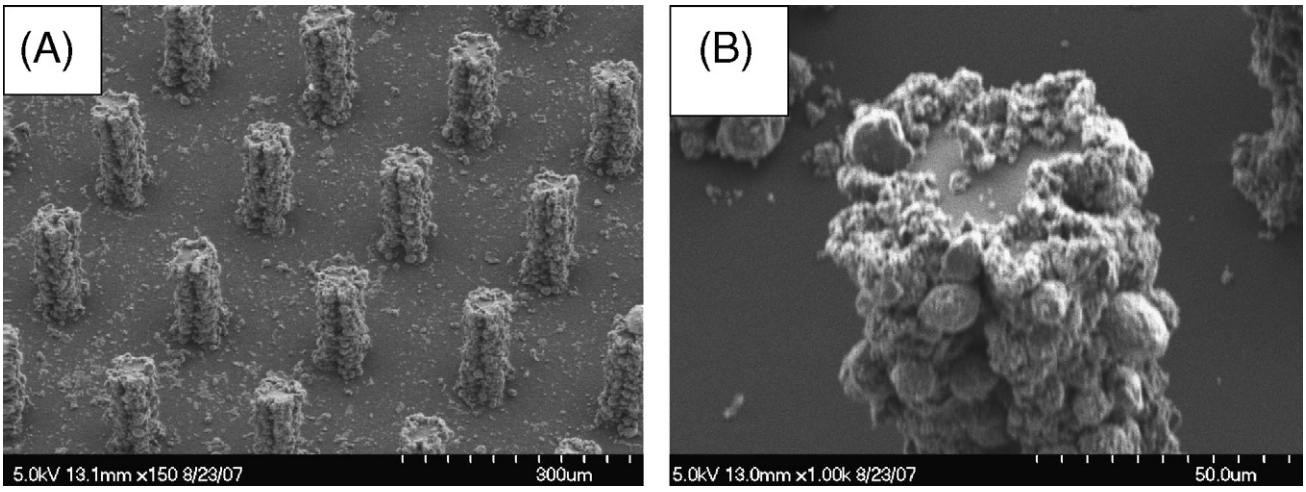

Fig. 3. Hybrid Carbon-MEMS/MCMB electrodes.

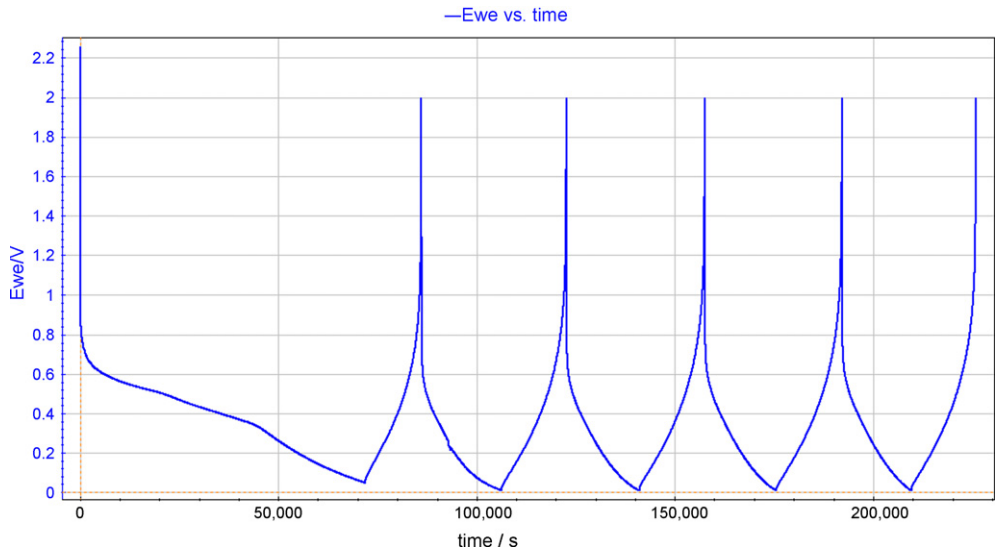

Fig. 4. Initial five charge/discharge experiments of a typical three-dimensional electrode. The voltage range is from 0.05 to 2 V.

To create the hybrid Carbon-MEMS/MCMB electrodes, we first fabricate the SU-8 microstructures using the process described above. The performance of two different solvents, *N*-methylpyrrolidone (NMP) and SU-8(2), to attach MCMB particles onto the patterned polymer has been evaluated. The first option was selected because NMP is a chemically stable and powerful polar solvent, widely used in the electronics industry and in the manufacturing of lithium-ion batteries. On the other hand, the SU-8(2) photoresist was chosen because, aside from the possibility of being used as solvent for the MCMB, it is possible to enhance the adhesion of the carbon particles onto the polymer microstructures by curing the dispersion with UV light, as it is done during the standard processing of SU-8 photoresist, after it has been coated over the high-aspect ratio microstructures. On the other hand, NMP holds the MCMB particles by London and van der Waals forces only.

When using NMP as solvent, a dispersion of MCMB on NMP at a concentration of 0.08 g ml^{-1} is prepared and spin coated onto the substrates at 2000 rpm for 40 s. The surface tension of NMP drags the particles to the surface of the polymer microstructures during evaporation. When using SU-8(2) as solvent, the MCMB particles are first dispersed in the photoresist at the same concentration as before. Then, the regular photoresist processing steps are followed in order to cross-link the monomer and firmly attach the MCMB particles onto the structure arrays. Afterwards, both types of hybrid structures are pyrolyzed.

3.3. Pyrolysis process

The entire process takes place in N_2 atmosphere (flow rate: 39.3 cm^3 s^{-1}) inside an alumina tube furnace (R.D. Webb Company, MA). The heating schedule is as follows:

- from 20 °C (room temperature) to 700 °C in 60 min;
- from 700 to 900 °C in 90 min;
- from 900 °C to the final pyrolysis temperature in 90 min;
- stay at the final pyrolysis temperature for 60 min;
- from the final pyrolysis temperature to 900 °C in 60 min;
- from 900 to 700 °C in 90 min;
- from 700 °C to room temperature in 300 min.

The final pyrolysis temperature is generally 1000 °C, but we have also studied the effect of this temperature on the reversible and irreversible capacities of the carbon anodes (see Section 4.2).

3.4. Electrochemical measurements

To test the performance of the carbon anodes, cells are assembled for characterization. In these electrochemical cells, the Carbon-MEMS samples are the working electrodes and lithium foil (0.75 mm thick, 99.9% purity, Aldrich) is used as counter electrode. Assembling of cells and tests are performed inside a glove box (Vacuum Atmospheres Co., CA) filled with argon (ultra-high purity grade, Airgas). The oxygen content of the chamber is kept at a concentration below 10 ppm. The samples are introduced inside the glove box immediately after pyrolysis to reduce the effects of condensation of water molecules on their surface, since condensation is known to reduce the overall performance of carbon electrodes [19]. The electrolyte used is a 1 M solution of lithium perchlorate ($LiClO_4$, 95+% purity, ACS grade) in a 1:1 (v/v) mixture of ethylene carbonate (EC, 99% purity) and dimethyl carbonate (DMC, 99+% purity), all from Sigma–Aldrich. A testing cell, made of polytetrafluoroethylene (PTFE), has been specially designed to host the samples. Micro-alligator clips (model BU-34, Mueller Electric) are used to contact the counter and working electrodes, and are polished with sand paper at every sample setup to reduce the Ohmic losses. The effective testing area of each cell is 0.654 cm^{-2}.

Galvanostatic (charge and discharge) experiments between 0.05 and 2 V are conducted at two different current densities, 76.4 and 152.7 μA cm^{-2}, using a multichannel potentio/galvanostat (VMP3, Princeton Applied Research). The first five charge/discharge cycles of one of the samples are shown in Fig. 4. Electrochemical impedance spectroscopy (EIS) experiments at 150 mV vs. Li/Li^+ were performed at the end of each charge/discharge routine to study the impedance of the electrode/electrolyte interface, the reaction kinetics of the lithium-ion intercalation process, and the formation of the solid-electrolyte interphase (SEI) at the surface of the carbon electrodes. The detailed parameters of the electrochemical testing routine are described in Table 2.

4. Results

4.1. Effect of structure density

To observe the relationship between the density of high-aspect ratio microstructures and the capacity of the electrodes, four different types of samples with increasing array density were

Table 2
Testing routine parameters

Routine name	Parameters
Soaking	3 h
Chronopotentiometry	76.4 μA cm^{-2} (half a cycle)
Electrochemical impedance spectroscopy (EIS)	200 kHz to 100 mHz, V_{pp} = 10 mV
Chronopotentiometry	76.4 μA cm^{-2} (6 cycles)
EIS	200 kHz to 100 mHz, V_{pp} = 10 mV
Chronopotentiometry	152.7 μA cm^{-2} (6 cycles)
EIS	200 kHz to 100 mHz, V_{pp} = 10 mV

Table 3
Properties of the carbon microstructure arrays—additional data used to obtain values on the table: carbon density: 1.7 g cm^{-3}; aspect ratio: 8:1; thickness of the underlaying carbon layer: 1.54 μm; sample area: 0.654 cm^{-2}

Sample type	Density of the array (microstructures mm^{-2})	Mass of carbon (g)	Surface area (mm^2)
Carbon layer	0	0.172	65.47
#1	27.8	0.630	98.25
#2	46.3	0.936	120.10
#3	68.9	1.309	146.76
#4	86.3	1.596	167.30

prepared. The geometric and gravimetric properties of the arrays, as compared to a plain carbon layer, are shown in Table 3.

The evolution of their lithium intercalation capacity over the first seven cycles is plotted in Fig. 5. It is worth noticing that the capacity stabilizes after very few cycles. The results of the lithium-ion intercalation tests for each one of these samples are shown in Figs. 6 and 7. Fig. 6 depicts the reversible and irreversible capacities of the electrodes as a function of the sample type, with the intercalation value normalized in terms of footprint of the sample. It is important to note that the current density is normalized to the footprint area of the cell (0.654 cm^{-2}), not to the total surface area of the Carbon-MEMS structures. In Fig. 7, the normalization is made in terms of the total mass of carbon present in each electrode, which gives their gravimetric capacity. The charts also show the reversible capacities of the carbon anodes at the two different current densities. Two samples of each type were tested, and the represented value is the average of the two quantities. The variances are not shown because only two data points are available for each test.

The irreversible capacity of the electrodes (see Fig. 6) is calculated as the difference between the first and the sixth charge cycle at a current density of 76.4 μA cm^{-2}. In all samples, the first intercalation capacity is larger than the first de-intercalation capacity. This difference is attributed to the formation of the SEI at the surface of the carbon electrode. Once the entire surface has been coated with this film, derived from the decomposition products of the electrolyte, further decomposition ceases, and the capacity of the electrode stabilizes at a constant value [20]. This decomposition reaction consumes a certain amount of charge that is not used to intercalate lithium ions into the carbon structure, and thus it is referred as the "irreversible" loss.

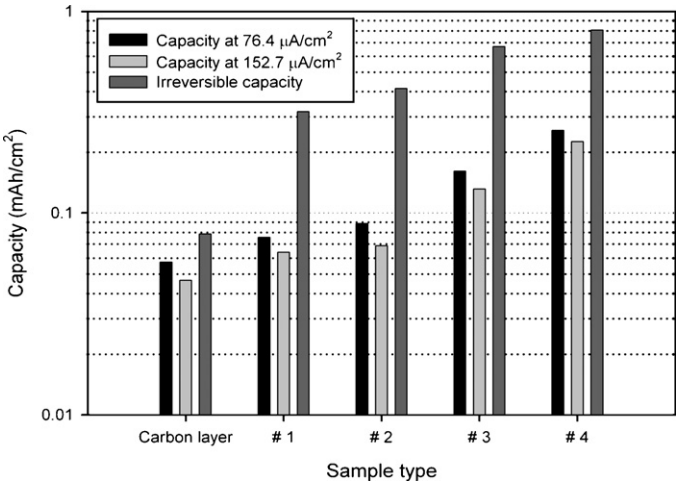

Fig. 6. Reversible and irreversible specific capacity of the Carbon-MEMS electrodes as a function of the microstructure array density.

4.2. Effect of pyrolysis conditions

As it is well reported in the literature, the overall physical and chemical properties of the carbon greatly depend, among other parameters, on the pyrolysis conditions [21]. To observe its consequences on the lithium-ion intercalation properties of the three-dimensional electrodes, we have tested their performance after variations in the pyrolysis conditions.

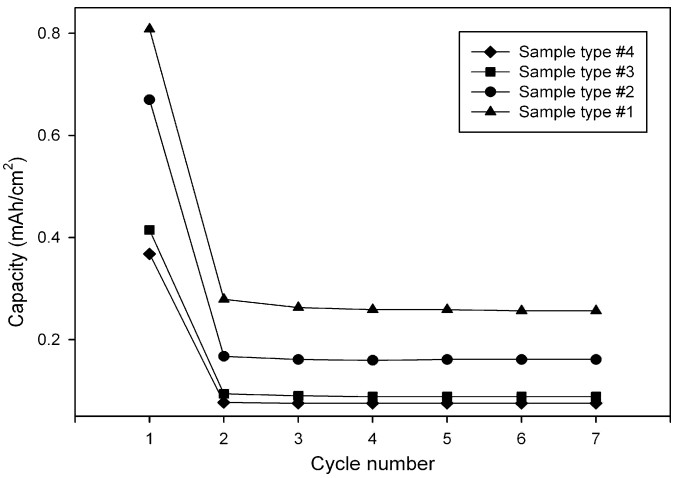

Fig. 5. Evolution of the lithium-ion intercalation capacity during the first seven cycles for samples with different microstructure array density.

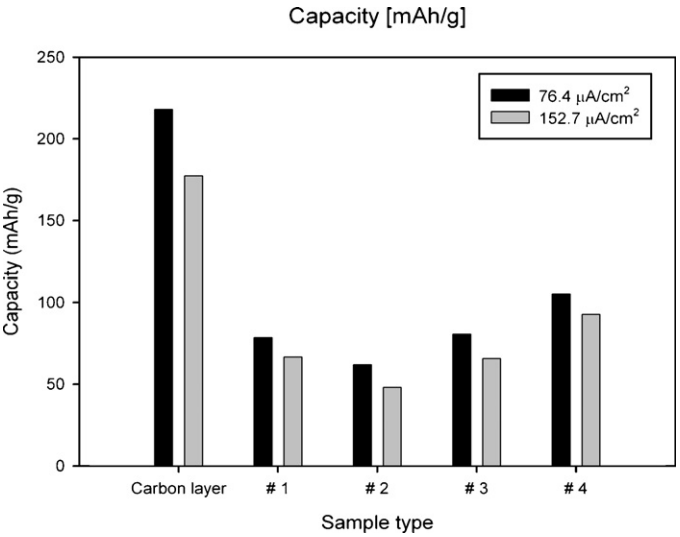

Fig. 7. Gravimetric reversible capacity of the Carbon-MEMS electrodes as a function of the microstructure array density.

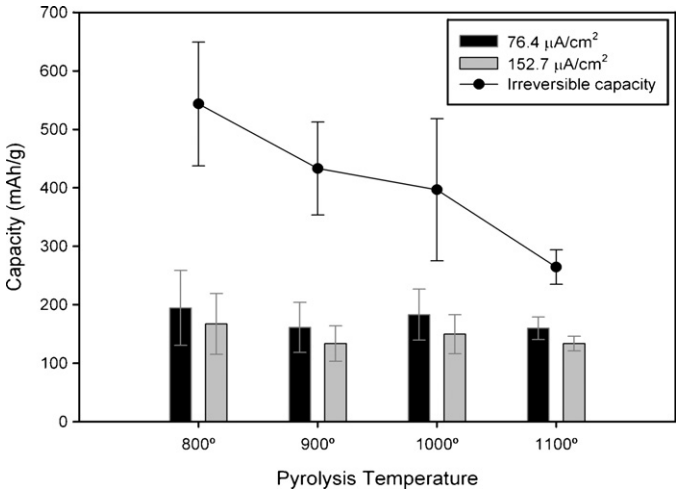

Fig. 8. Effect of the final pyrolysis temperature in the specific capacity.

4.2.1. *Effect of the final pyrolysis temperature*

The first study involves observing the relationship between the final pyrolysis temperature and the total intercalation capacity of carbon films. In order to reduce variations in capacity due to uneven film thicknesses, all films were prepared on the same substrate and then pyrolyzed at different temperatures. The heating schedule is shown in Section 3.3, the only difference between samples being the final temperature: 800, 900, 1000 or 1100 °C. Four samples of each type were tested, so the standard deviation of the intercalation values is reported. The data is normalized in gravimetric terms (we assume that the density of the carbon films does not significantly change with the pyrolysis temperature). The results are shown in Fig. 8.

4.2.2. *Effect of the pyrolysis temperature profile*

Another interesting parameter to study is the effect of the pyrolysis temperature profile over the reversible and irreversible capacities of the electrodes. For this purpose, two different heating schedules have been tested, which represent variations over the previous heating program shown in Section 3.3. In the first variation, the final temperature of 1000 °C is held for 5 h, while keeping all the other heating times as in the initial tests. In the second variation, the ramping schedule has been modified by extending the initial heating process, especially between 300 and 600 °C. This interval has been chosen because the evolution from SU-8 photoresist to carbon occurs mostly within this temperature range, as it has been reported using thermo-gravimetric analysis [22]. In this case, the heating schedule is

- from 20 °C (room temperature) to 300 °C in 60 min;
- from 300 to 600 °C in 300 min;
- from 600 to 900 °C in 180 min;
- from 900 to 1000 °C in 60 min;
- hold at 1000 °C for 60 min;
- from 1000 to 700 °C in 180 min;
- from 700 °C to room temperature in 180 min.

For simplicity, only sample types #1 and #2 were tested. The results of the intercalation capacities of the new samples are plotted in two different graphs, normalized in terms of area (Fig. 9) and mass (Fig. 10), and compared to the initial intercalation results. The irreversible capacity is shown in Fig. 11. In this case the percentage of the reversible capacity is calculated as follows: [% = (irrev. − rev.)/rev. × 100].

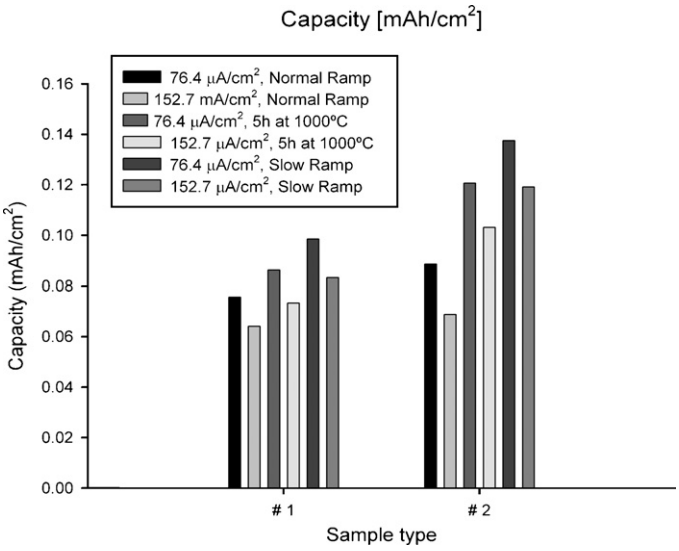

Fig. 9. Effect of the pyrolysis temperature schedule in the specific capacity.

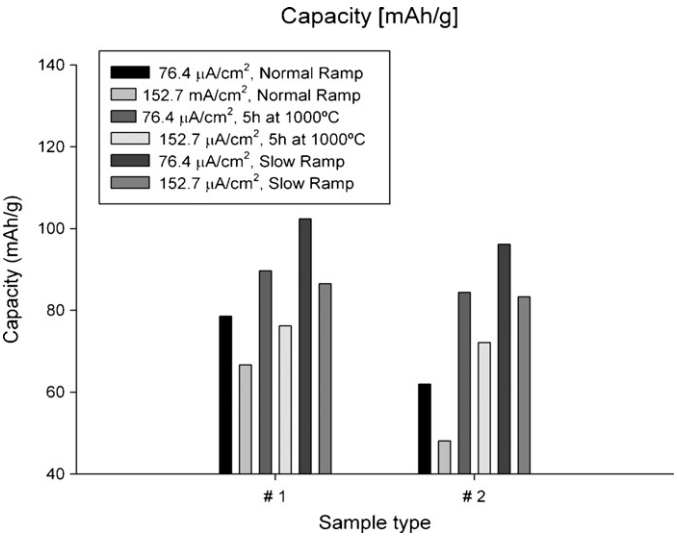

Fig. 10. Effect of the pyrolysis temperature schedule in the gravimetric capacity.

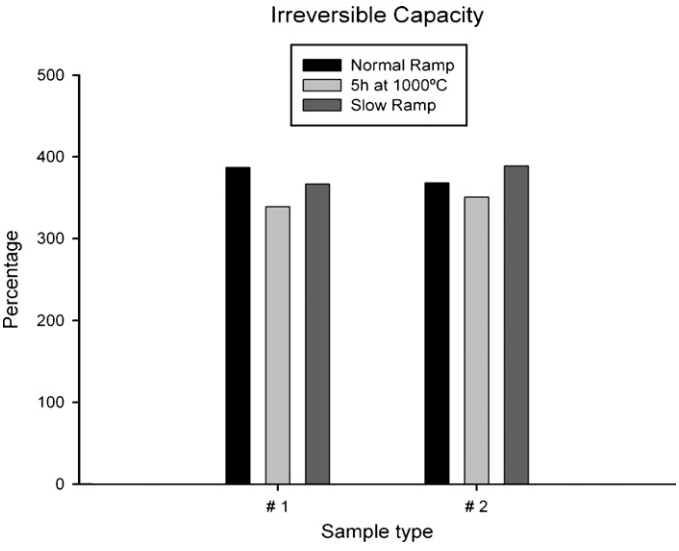

Fig. 11. Effect of pyrolysis program in the irreversible capacity.

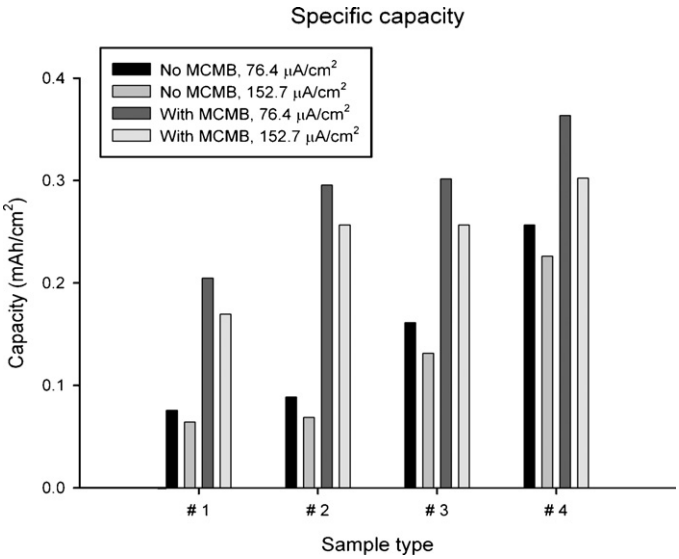

Fig. 12. Specific capacity of C-MEMS electrode with and without MCMB particles.

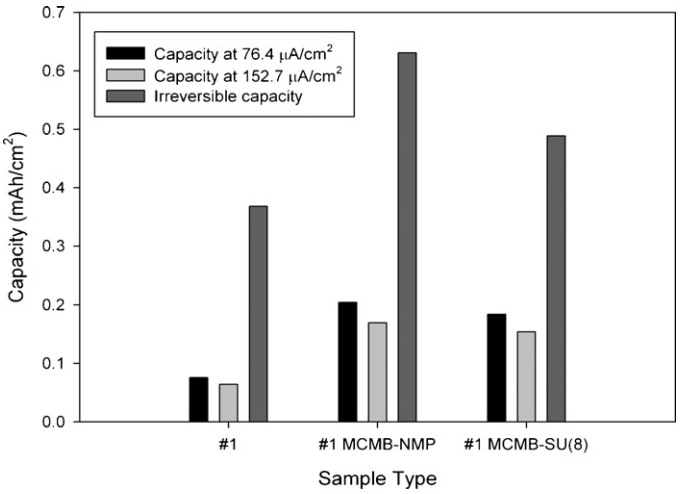

Fig. 14. Comparison of the intercalation capacity normalized per footprint area of the samples without MCMB (left), with MCMB attached with NMP (center) and with MCMB attached with SU-8(2) (right). In all cases, the microstructures were of the same height and pyrolyzed under the same conditions. The irreversible capacity is represented in the same plot.

4.3. Effect of MCMB addition to the Carbon-MEMS anodes

The capacity – normalized in terms of footprint area – of the hybrid Carbon-MEMS/MCMB electrodes at two different current densities is represented in Fig. 12. In the same graph, the performance of the samples without MCMB particles is also represented for comparison. The gravimetric normalization of the capacity of these samples has not been obtained because the exact mass of carbon contributed by the MCMB particles was unknown. As in the earlier instances, the percentage of irreversible capacity has been measured, and is presented in Fig. 13.

The samples in which the MCMB is attached with SU-8(2) photoresist undergo dramatic failure during the pyrolysis process, making them totally unusable for the lithium-ion intercalation tests. Only sample type #1 survives the process. The reason for this failure is related to the unequal coefficients of thermal expansion of carbon and silicon: cracking and separation occurs because the photoresist shrinks during its conversion into carbon while the silicon substrate's dimension change is relatively insignificant. The photoresist added to the samples to attach the MCMB particles causes more stress to be built up at the carbon/silicon interface. This ultimately results in mechanical failure of the carbon structures. The samples with more array density can retain more photoresist between the microstructures, which ultimately causes them not to survive the pyrolysis process. Nevertheless, the two successful samples of type #1 are tested and compared to the ones fabricated using NMP (see Fig. 14).

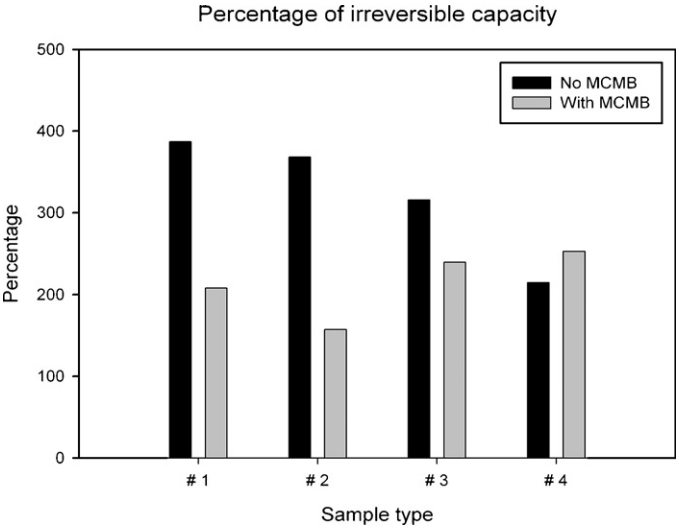

Fig. 13. Comparison in the percentage of irreversible capacity in the samples with and without MCMB.

5. Discussion

5.1. Carbon-MEMS electrodes

5.1.1. Reversible capacity

We first analyze the specific and gravimetric capacities of the five initial samples (the carbon layer and the four array densities). When the data is normalized in terms of specific (areal) capacity (Fig. 6), we observe that the total capacity increases with the array density. As expected, the samples, ordered from carbon layer to sample #4, have an increasing amount of carbon within the same footprint and therefore there are more sites for the lithium ions to intercalate, which accounts for the increase in total capacity. On the other hand, when we normalize in gravimetric terms (Fig. 7) we observe a rather unexpected behavior. If the carbon of all samples had been able to intercalate the same amount of lithium, we would have obtained the same capacity on every experiment. Instead, the gravimetric capacity is much lower for the samples with carbon microstructures than for the carbon layer. Possible explanations for this situation are:

(1) The resulting thickness of the carbon structures (17 μm) is too large for the lithium ions to diffuse into the entire cross-section of the structure, and therefore not all the carbon is used as intercalation material. The carbon layer, on the other hand, being only 1.5 μm thick, is capable of fully intercalating ions throughout its entire cross-section.
(2) Using the same current density per footprint of material on the different samples corresponds to having a different current densities per unit of area on each sample, because the total surface area of the samples is different. This affects the kinet-

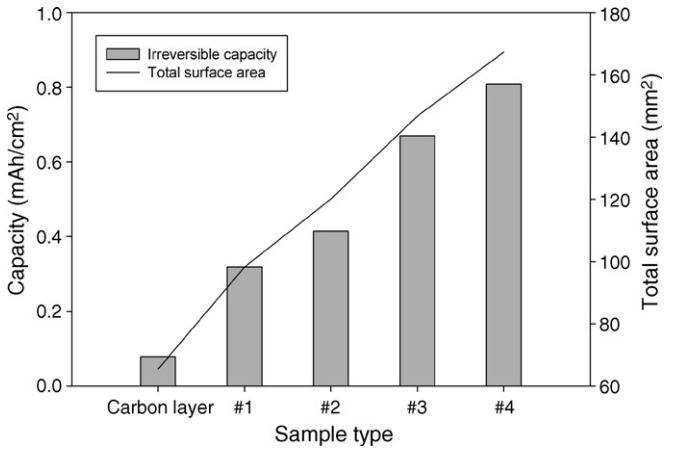

Fig. 15. Absolute values of the irreversible capacity of the different samples (bar) and the total area of the electrodes (line).

ics of the intercalation reaction in samples that have very large surface areas, as in the case of samples with C-MEMS structures.

Even though the relative contribution of these two effects is not exactly known, it is reasonable to think that the most notable contribution to the loss of gravimetric capacity is the first one. A possible solution for this problem would be to fabricate structures with thinner structural components, which would also contribute to obtaining a final battery with faster charge/discharge kinetics.

5.1.2. Irreversible capacity

As it is shown in Fig. 6, the irreversible capacity is much larger in the samples with Carbon-MEMS structures than on the plain carbon layer. Dahn and co-workers were the first researchers to correlate the irreversible capacity loss (Q_{irr}) with the capacity required for the formation of the SEI. They found that Q_{irr} is proportional to the specific surface area of the carbon electrode [23]. Indeed if we plot the irreversible capacity and the total surface area of the samples in the same graph (Fig. 15), it is clear that the irreversible capacity follows to a high extent the curve of the total area on each sample.

The study of the formation of the SEI layer on photoresist-derived carbon layers has already been investigated in great detail by the Madou and co-workers [20]. However, Q_{irr} may have other sources as well, such as the unused capacity under specified experimental conditions (available using low current rates and high potentials), or capacity losses associated with the trapping of lithium inside the structure of carbon, generally as a result of irreversible reactions of the lithium ions with impurities present on the inner surface of closed pores [24]. A behavior that is slightly more complex to justify is that of the irreversible capacity (Fig. 6). In this case we see that the irreversible capacity is around six times larger in samples with carbon structures than in the carbon layer. This effect can be reasoned as follows: the irreversible capacity depends on the surface area, whereas the reversible capacity is dependent on the amount of carbon (intercalation sites for lithium ions). Since we are not using the full intercalation capability of the carbon in the samples with Carbon-MEMS structures (as seen in the previous section), the percentage of irreversible capacity is much higher in all of them, because the total surface area, where the SEI formation occurs, is much larger in the samples with three-dimensional carbon structures as compared to the carbon layer.

5.2. C-MEMS electrodes with MCMB

5.2.1. Reversible capacity

The graph shown in Fig. 12 demonstrates that the combined C-MEMS/MCMB electrodes have a larger specific capacity than the samples without carbon particles, mostly because there is more carbon deposited on the electrodes. It is worth noticing that the reversible capacity of the samples in which the particles have been attached with SU-8(2) is lower than the NMP case, which demonstrates that fewer particles are deposited onto the structure—the amount of carbon contributed by the pyrolysis of the solvent (SU-8(2)) plus the MCMB is still smaller than the MCMB alone in the case where we use NMP as solvent.

It would have been extremely interesting to have measured the mass of carbon on each type of hybrid electrode to obtain their gravimetric capacity, but this has not been possible because the difference in weight between the plain Carbon-MEMS electrodes and the ones coated with MCMB particles is so small that it cannot be resolved with the weighing scale available in our laboratories (0.1 mg resolution). This data would have shed light onto the extent of utilization of the carbon particles at the electrodes, as well as the quality of the attachment between them and the carbon structures. Conveniently enough, this information can be extracted from the analysis of the irreversible capacity.

5.2.2. Irreversible capacity

In Fig. 13 we can observe the evolution of the percentage of irreversible capacity with and without MCMB particles in all four types of samples when using NMP as solvent. For types #1 and #2 (the less dense arrays), the percentage is much higher in the samples without MCMB than in plain Carbon-MEMS structures. On the other hand, samples #3 and #4 have a very similar percentage of irreversible capacity. This behavior can be ascribed to the quality of the adhesion of the carbon particles to the structure. In the low array density samples (#1 and #2) the MCMB create a conformal coating at the surface of the C-MEMS posts, with no particles being loose or misplaced. On the contrary, in samples #3 and #4 the coating of particles is not as uniform, and the particles aggregate and form bundles due to the higher density of the array. In this case, the detachment of MCMB particles during the charge and discharge cycling of the carbon electrode is linked to the increased irreversible capacity.

The conjecture of the detachment of MCMB particles is based on two observations: first, when the battery testing cells are disassembled, it is possible to observe some of the MCMB particles dispersed in the electrolyte solution. These particles may have contributed to the initial charging capacity but, after being detached from the substrate, they no longer contribute to the intercalation of lithium ions, thereby increasing the irreversible capacity. Second, samples in which SU-8(2) is used as solvent for MCMB attachment, have a slightly smaller percentage of irreversible capacity (see Fig. 14) which can be attributed to the better attachment of MCMB.

5.3. Electrode kinetics

To study the effect of the MCMB deposition method on the electrode kinetics, it is convenient to observe the electrochemical impedance spectroscopy plots for each sample type (Fig. 16). In all three cases we observe that the charge transfer resistance (R_{ct}) increases after the first charge/discharge curve. This is a consequence of the SEI layer formation, which reduces the ion transfer kinetics at the electrode/electrolyte interface. The major qualitative difference, though, is observed at the end of the charge/discharge cycles at 157 $\mu A\,cm^{-2}$. In the samples with MCMB particles, R_{ct} keeps increasing, which confirms that the build

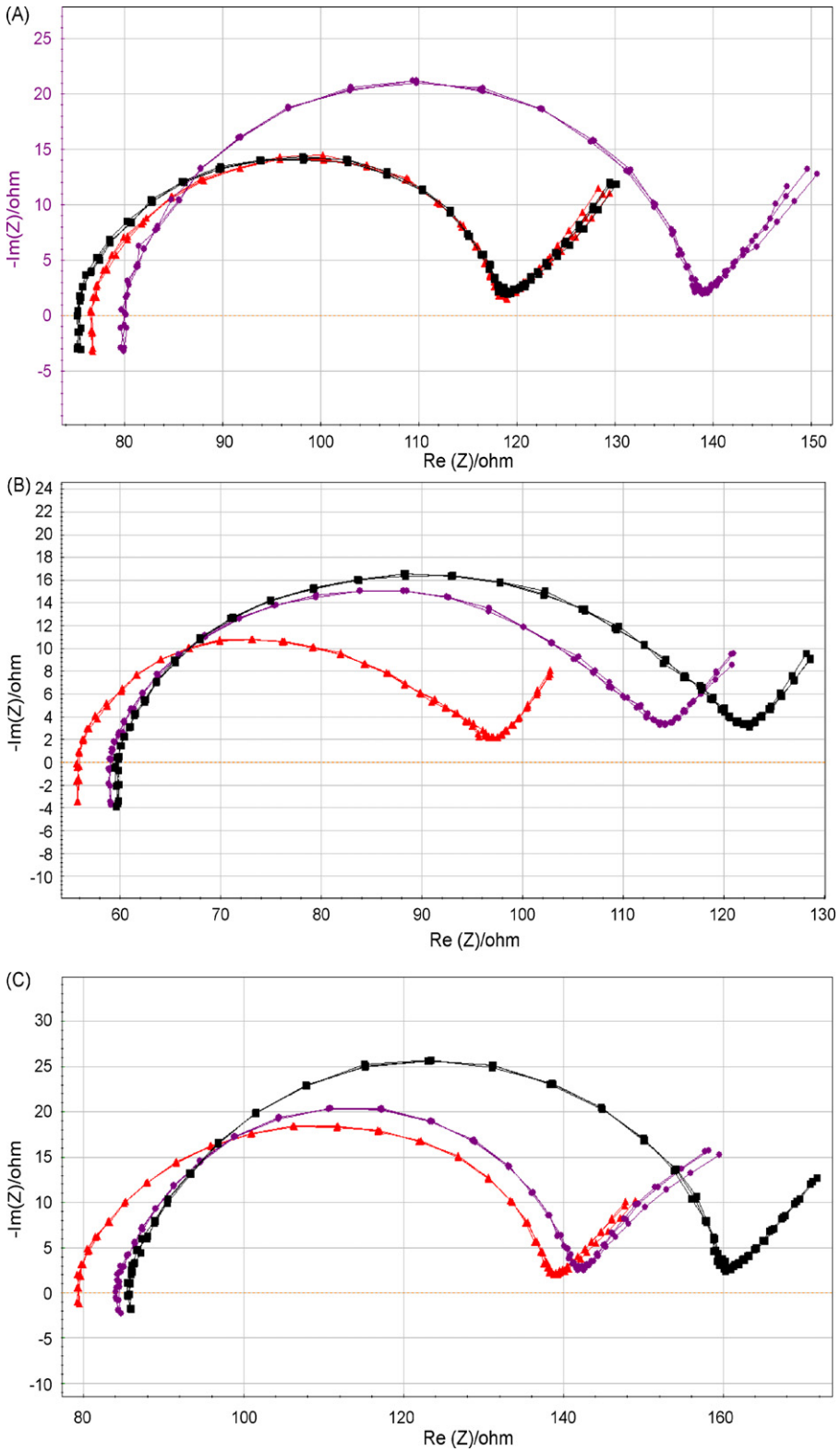

Fig. 16. Electrochemical impedance spectroscopy results for each type of coating. (A) No MCMB, (B) MCMB/NMP and (C) MCMB/SU-8(2). The sample type is #1 in all the plots. Triangles: EIS after first charge. Squares: EIS after 6 charge/discharge cycles at 76.4 $\mu A\,cm^{-2}$. Circles: EIS after 6 charge/discharge cycles at 152.7 $\mu A\,cm^{-2}$.

up of the SEI layer continues after the first 12 charge/discharge cycles (6 at 76.4 $\mu A\,cm^{-2}$ and 6 at 152.7 $\mu A\,cm^{-2}$). On the other hand the plain Carbon-MEMS sample has a reduction in the R_{ct} value because the total surface area or the plain Carbon-MEMS sample is much lower than that of the samples with MCMB, and thus there is less SEI layer formation over time. That, in turn, reduces and stabilizes the charge transfer resistance after the first 12 cycles.

5.4. Pyrolysis process

5.4.1. Variation in the final temperature

It is clear from Fig. 8 that increasing the final pyrolysis temperature reduces the irreversible capacity of carbon films while maintaining the same reversible capacity. Even though most of the irreversible losses are attributed to the formation of the SEI, with this experiment we can conclude that this is not the only contribution to it. The carbon films used in these tests have almost atomically smooth surfaces, as observed with atomic force microscope. This means that the total surface area that is exposed to the electrolyte, and thus to SEI formation, is the same in all samples. Since we also use the same experimental conditions in all cases, we infer that the losses due to SEI formation are equal for each one of the carbon films. What is the origin of the different irreversible capacity, then? The most plausible explanation is that the elemental composition of the carbon in the four samples is slightly different. When pyrolyzing at different temperatures, the decomposition of the polymeric material leads to carbons with different chemical composition [12,13]. The general understanding is that at lower temperatures, more oxygen and hydrogen atoms are present in the carbon films. These, in turn, are known for binding lithium ions irreversibly (especially hydrogen); once lithium is intercalated into the carbon film, its interaction with hydrogen and oxygen atoms obstructs its de-intercalation, thereby contributing to the observed irreversible capacity. On the other hand, thermodynamic calculations done by Benzinger and Huttinger show that at 1000 °C, any hydrocarbon will be almost completely decomposed into hydrogen and carbon [25,26]. This may account for the reduced irreversible capacity of the samples pyrolyzed at 1000 and 1100 °C. In these cases, most of the irreversible capacity is attributed to the SEI formation.

5.4.2. Variation in the heating profile

In Figs. 9 and 10 we represented the effect of the pyrolysis temperature schedule in the specific and gravimetric reversible capacities of the C-MEMS electrodes. The plots show that heating the samples at lower rates has more of an influence on reversible capacities than holding the final pyrolysis temperature for a longer time. Given the fact that the samples have the same geometries, this effect has to be explained from the point of view of the material composition: slower heating rates allow for a better outgassing of the non-carbonizing compounds at the initial stages of the pyrolysis process, as well as a better build up of the carbon crystalline structure that hosts lithium ions. With respect to the irreversible capacity, we can see in Fig. 11 that it has approximately the same value in all samples. In this case, the relative contribution of the carbon composition to the irreversible capacity is less important than in the case of carbon films because of the large surface area of the three-dimensional structures (the SEI formation is related to the total surface area of the carbon electrode). Therefore, the heating rate does not play a substantial role in the irreversible capacity of the carbon electrodes.

6. Conclusions

The conclusions that can be drawn from the study of the new three-dimensional carbon anodes are:

(1) The three-dimensional architecture has a clear advantage in applications where the footprint of the battery is critical. This new approach achieves 3–6 more specific capacities than its thin-film counterparts.
(2) The cross-shaped C-MEMS arrays have a much higher mechanical robustness (as given by their moment of inertia) than the traditionally used cylindrical posts, but the dimensions of the structures used in this study are too large to allow the lithium ions to diffuse into the core of the carbon structure, as seen by the reduction of the gravimetric capacity of the C-MEMS anodes with respect to the carbon layers. New designs with thinner features are required for better carbon utilization.
(3) Addition of MCMB particles has an overall positive effect in the reversible capacity of the new three-dimensional electrodes, but the big increase in irreversible capacity due to the lack of satisfactory attachment of carbon particles and the slower reaction kinetics due to increase in surface area shadow their advantages.
(4) The pyrolysis temperature schedule is key to controlling the properties of the resulting carbon. Even though the precursor (an epoxy resin) always results in a hard (non-graphitizing) carbon, pyrolyzing at higher temperatures and doing a slower ramping up schedule reduces the irreversible capacity of the carbon electrodes.

Modern microlithography allows for the fabrication of essentially any envisioned electrode and cell geometry. It is clear that while significant increases in both power and areal energy capacity are obtainable from 3D microbatteries, the inherent difficulty in the fabrication may limit the wide spreading of the use of such devices, especially in an environment that works with very small cost margins such as the battery market. With almost total certainty the use of this type of batteries will be limited to highly specialized, value-added applications.

Modeling the overall current–voltage behavior of three-dimensional cells is a complex task that depends on many factors (ionic and electronic conductance, interfacial reaction kinetics, charge capacity, etc.). This is an aspect that we have not treated in this contribution, but that will be a rich field of study for electrochemical engineers and will likely lead to new design concepts in battery technology. A delicate balance of the geometrical length scales (electrode radius and length, and the spacing between electrodes) and materials properties will be required during the optimization process.

Acknowledgments

This work was supported through a sponsored research agreement by Carbon Micro Battery, LLC, and was supported by the National Science Foundation under Grant No. CBET-0709085.

References

[1] J.M. Tarascon, M. Armand, Nature 414 (2001) 359–367.
[2] M. Wakihara, O. Yamamoto (Eds.), Lithium Ion Batteries: Fundamentals and Performance, Kodansha Ltd. and Wiley–VCH Verlag GmbH, 1998.
[3] J. Bates, N. Dudney, B. Neudecker, A. Ueda, C. Evans, Solid State Ionics 135 (2000) 33–45.
[4] http://www.oakridgemicro.com/tech/tfb.htm.
[5] J. Long, B. Dunn, D. Rolison, H. White, Chem. Rev. 104 (2004) 4463–4492.
[6] G. Baure, C.W. Kwon, G.G. Lee, F. Chamran, C.J. Kim, B. Dunn, Micropower and Microdevices, Electrochemical Society, Pennington, NJ, 2002.
[7] Y. Shao-Horn, C. Hidrovo, S.M. Jurga, H.I. Smith, G. Barbastathis, Proceedings of the Abstracts of the 204th Meeting of the Electrochemical Society, Pennington, NJ, 2003 (Abstr.#1279).
[8] M. Madou, A. Lal, G. Schmidt, X. Song, K. Kinoshita, M. Fendorf, A. Zettl, R. White, Electrochemical Society Proceedings '97, 1997, pp. 61–69.
[9] G. Turon Teixidor, C. Wang, M. Madou, Proceedings of theNSTI Nanotechnology Conference, Boston, MA, 2006.
[10] I. Jafri, H. Busta, S. Walsh, SPIE Proceedings, 3880, 1999, pp. 51–58.
[11] US Patent #4,882,245.
[12] R. Kostecki, B. Schnyder, D. Alliata, X. Song, K. Kinoshita, R. Kötz, Thin Solid Films 396 (2001) 36–43.

[13] S. Ranganathan, R. McCreery, S.M. Majji, M. Madou, J. Electrochem. Soc. 147 (2000) 277–282.
[14] Y. Liu, J. Xue, T. Zheng, J. Dahn, Carbon 34 (1996) 193–200.
[15] B. Park, L. Taherabadi, C. Wang, J. Zoval, M. Madou, J. Electrochem. Soc. 152 (2005) J136–J143.
[16] Ch. Wang, L. Taherabadi, G. Jia, M. Madou, Y. Yeh, B. Dunn, Electrochem. Solid State Lett. 7 (2004) A435–A438.
[17] J. Yao, G. Wang, J. Ahn, H. Liu, S. Dou, J. Power Sources 114 (2003) 292–297.
[18] J.O. Besenhard (Ed.), Handbook of Battery Materials, Wiley–VCH Verlag GmbH, 1999.
[19] K. Kinoshita, Carbon: Electrochemical and Physicochemical Properties, Wiley-Interscience, 1988.
[20] F. Galobardes, C. Wang, M. Madou, Diamond Relat. Mater. 15 (2006) 1930–1934.
[21] G.M. Jenkins, K. Kawamura (Eds.), Polymeric Carbons—Carbon Fiber, Glass and Char, Cambridge University Press, 1976.
[22] A. Singh, J. Jayaram, M. Madou, S. Akbara, J. Electrochem. Soc. 149 (2002) E78–E83.
[23] R. Fong, U. Sacken, J. Dahn, J. Electrochem. Soc. 137 (1990) 2009–20013.
[24] W. Xing, J. Dahn, J. Electrochem. Soc. 144 (1997) 1195–1201.
[25] W. Benzinger, A. Becker, K.J. Huttinger, Carbon 34 (1996) 957–966.
[26] W. Benzinger, K.J. Huttinger, Carbon 34 (1996) 1465–1471.